IEEE Access
Multidisciplinary : Rapid Review : Open Access Journal

Received July 25, 2020, accepted August 1, 2020, date of publication August 12, 2020, date of current version August 31, 2020.

Digital Object Identifier 10.1109/ACCESS.2020.3016004

A Hybrid Fusion Strategy for the Land Vehicle Navigation Using MEMS INS, Odometer and GNSS

SHUANG DU[1,2], SHU ZHANG[3], AND XUDONG GAN[1,2]

[1]School of Aeronautics and Astronautics, University of Electronic Science and Technology of China, Chengdu 611731, China
[2]Aircraft Swarm Intelligent Sensing and Cooperative Control Key Laboratory of Sichuan Province, University of Electronic Science and Technology of China, Chengdu 611731, China
[3]Sichuan Jiuzhou Electric Group Company Ltd., Mianyang 621000, China

Corresponding author: Shuang Du (sdu@uestc.edu.cn)

This work was supported in part by the National Natural Science Foundation of China under Grant 41704029; and in part by the Sichuan Province Science and Technology Project under Grant 2018CC0018, Grant 2018GZDZX0013, and Grant 2018SZ0364.

ABSTRACT How to limit the drifts of the navigation errors in an inertial navigation system (INS) with low-cost sensors is one of the main challenges for the land vehicle navigations. In this paper, we present a novel hybrid navigation strategy to integrate the Micro-Electric-Mechanic-systems (MEMS) INS, odometer (OD) and global navigation satellite systems (GNSS), with aim to enhance the positioning accuracy of the inertial system during GNSS outages. To accurately estimate the INS error states, the neural network (NN) is proposed to mimic the velocity of the navigation frame with the data from the MEMS INS, odometer, as well as the non-holonomic constraints (NHC). The long short-term memory (LSTM) NN is adopted in our approach due to its ability to adaptively use the data in the past. The road tests are conducted with two different MEMS IMUs to verify the proposed navigation strategy. Comparing to the traditional integrated MEMS INS/OD/GNSS system based on the extended Kalman filtering (EKF), our hybrid approach provides over 60% improvements in terms of the root mean square (RMS) and maximum horizontal position errors during GNSS outages.

INDEX TERMS Artificial intelligence, global navigation satellite system, inertial navigation, sensor fusion, parameter estimation.

I. INTRODUCTION

The strapdown inertial navigation system (INS) usually consists of a triad of accelerometers and gyroscopes, which measures the vehicle's acceleration and rotation rate with respect to the inertial frame. A set of mathematical transformations and integrations with respect to time are applied to the inertial measurements to calculate the position, velocity and attitude information. The main drawback of INS is that the navigation errors, including position, velocity and attitude errors accumulate over time because of the intrinsic property of dead reckoning [1]. Due to the merits of low-cost, small-size and low power-consumption [2], the Micro-Electric-Mechanic-systems (MEMS) inertial sensors have been widely employed for the land vehicle navigations. However, they feature significant sensor errors, such as high-frequency noise, bias instability and misalignment errors [3], [4]. As a result, the navigation errors grow dramatically for an MEMS INS. To eliminate the error accumulations of an inertial system, the global navigation satellite systems (GNSS) was widely employed, and the Kalman filtering (KF) is the most popular technique to fuse the GNSS and INS data. In such integrated systems, the GNSS position and velocity are used as measurements to estimate the INS position, velocity and attitude errors, as well as the inertial sensor errors [5]–[7]. However, the GNSS signals are easily to be blocked when the vehicle travels through urban areas or tunnels, then the navigation errors still accumulate when the INS works in standalone mode during GNSS outages. Typically, the position errors accumulate to hundreds of meters in tens of seconds for the MEMS INS [8], [9].

Because of the advantages in nonlinear mapping between inputs and outputs without the pre-defined mathematical model [10]–[12], the artificial neural networks (ANN) were proposed to reduce the INS navigation errors during GNSS outages. A brief summary of related research is introduced as follows. The position update architecture (PUA) was proposed with the multiplayer perceptron (MLP) neural

The associate editor coordinating the review of this manuscript and approving it for publication was Huiyu Zhou.

This work is licensed under a Creative Commons Attribution 4.0 License. For more information, see https://creativecommons.org/licenses/by/4.0/

networks to predict the position increment over time with the inputs of the INS velocity and azimuth [13]. When the GNSS is available, the neural network is trained with the GNSS-derived position increments, while it is used to predict them based on the INS outputs during GNSS outages. More complex architectures, which incorporate the prediction of vehicle velocity or azimuth, were also designed and proved to be able to offer better positioning performance [14], [15]. The limitation of MLP is that it is difficult to determine the optimal internal structure, such as number of layer and number of neurons in each layer [13]. Other than predicting the position increments, the $P - \delta P$ model and $V - \delta V$ model were proposed to mimic the INS position and velocity errors with inputs of INS position and velocity, respectively. The employed neural networks includes radial basis function (RBF) [16], [17], adaptive neuro-fuzzy inference system (ANFIS) [18]–[21] and the input-delayed neural networks (IDNN) [22]. Comparing to the MLP, the RBF could dynamically generate the internal structure to achieve the best system performance [23]. ANFIS shows advantages in dealing with the imprecision, uncertainty, and high level of stochastic of input data in nonlinear dynamic environments [24], however its parameter optimization leads to an enormous computational burden and long design time [18], [19]. By using the input-delayed mechanism, the IDNN is able to take the past samples into account. In addition to the INS velocity and attitude, the raw measurements from inertial sensors are also added as inputs, and different learning algorithms, such as ensemble learning algorithm [25] and back propagation (BP) with stochastic gradient descent (SGD) algorithm [26] are employed in the training procedures. The hybrid approaches of integrating KF and neural network were also studied. The neural network aided KF was proposed for the integration of INS and GPS, in which the neural networks is employed to identify the system states and measurement covariance matrix in real time [27], [28]. Moreover, the neural networks were trained to predict the KF error states with inputs of the vehicle dynamic variations during GNSS outages [29].

The random errors of the inertial system (such as the noise and bias instability) may cause the inconsistency to the pre-trained ANN model, which deteriorate its prediction accuracy. Therefore, the ANN-based approaches can only partially compensate the INS navigation errors, and the residual errors still accumulate over time [16]–[22]. Moreover, due to the high-level noise and bias instability of the MEMS inertial sensors, the ANN has shown a very limited success when applied to a MEMS INS [30]. As a result, aiding sensors are still required to further limit INS error drift during GNSS outages. The odometer (OD) is one of the most common sensors used for the land vehicle navigation, and the integrated INS/GNSS/OD system was usually proposed, in which the forward velocity derived from the odometer can be used to control the INS error drifting during GNSS outages [30]–[32]. The estimation approaches includes the federated KF [30], the extended KF [31], [32] and the particle filter [33]. The measurements of the GNSS position and velocity derived in the navigation frame directly provide the estimates of the INS position and velocity error states, which maintains system positioning accuracy. Moreover, the aiding odometer data also contribute to the attitude estimation [34]. During GNSS outages, only the forward velocity measurements are available to estimate the INS error states, which leads to the reduced stochastic observability of the position and velocity errors. As a result, the position and velocity solution still drift over time, which remains as a challenge for the land vehicle navigations.

In this paper, we aim to enhance the positioning performance of the MEMS INS during GNSS outages by proposing a hybrid navigation strategy to integrate the MEMS INS, odometer and GNSS based on both of the Kalman filtering and neural networks. When GNSS is available, the navigation data from the inertial system, odometer and GNSS is fused with an extended KF. Meanwhile, a neural network is proposed to mimic the velocities in the east and north directions of the navigation frame to accurately estimate the INS error states during GNSS outages. The inputs include the MEMS INS data, odometer data, and the nonholonomic constraints (NHC), which assumes the velocity components in the upward and transverse axes are zeroes for land vehicles when they run normally [35]–[38]. Due to the ability to adaptively use the data in the past [39], the long short-term memory (LSTM) neural network (NN) is employed in our approach. Comparing to the traditional neural networks, the LSTM NN shows the advantage in modelling the time correlated sequential data, as it is able to memorize the long-term dependencies of the sequential data. The road tests are conducted with two different MEMS IMUs, namely NAV440 and Crista, to verify the proposed navigation strategy. Comparing to the traditional integrated MEMS INS/OD/GNSS system based on the extended KF, our hybrid approach provides over 60% improvements in terms of the root mean square (RMS) and maximum horizontal position errors during GNSS outages.

The remainder of this paper is organized as follows. Section 2 introduces the overall navigation strategy with the system flowchart. Section 3 presents the integrated MEMS INS/OD/GNSS systems based the extended KF with focus on the data fusion algorithm and the system error analysis from analytic point of view. The proposed LSTM NN to derive the velocity of navigation frame is given in Section 4, followed by the road tests and results analysis present in Section 5. Finally, the conclusions are summarized in Section 6.

II. PROPOSED HYBRID NAVIGATION STRATEGY

Figure 1 illustrates the flowchart of the proposed hybrid navigation strategy, which works in two different modes related to the GNSS availability. When GNSS signals are available, the hybrid system works in the training mode, where the MEMS INS, odometer and GNSS are integrated based on the EKF as shown in (a). The ANN is proposed based on the LSTM to predict the velocities in the east and north directions of the navigation frame with the inputs being the specific

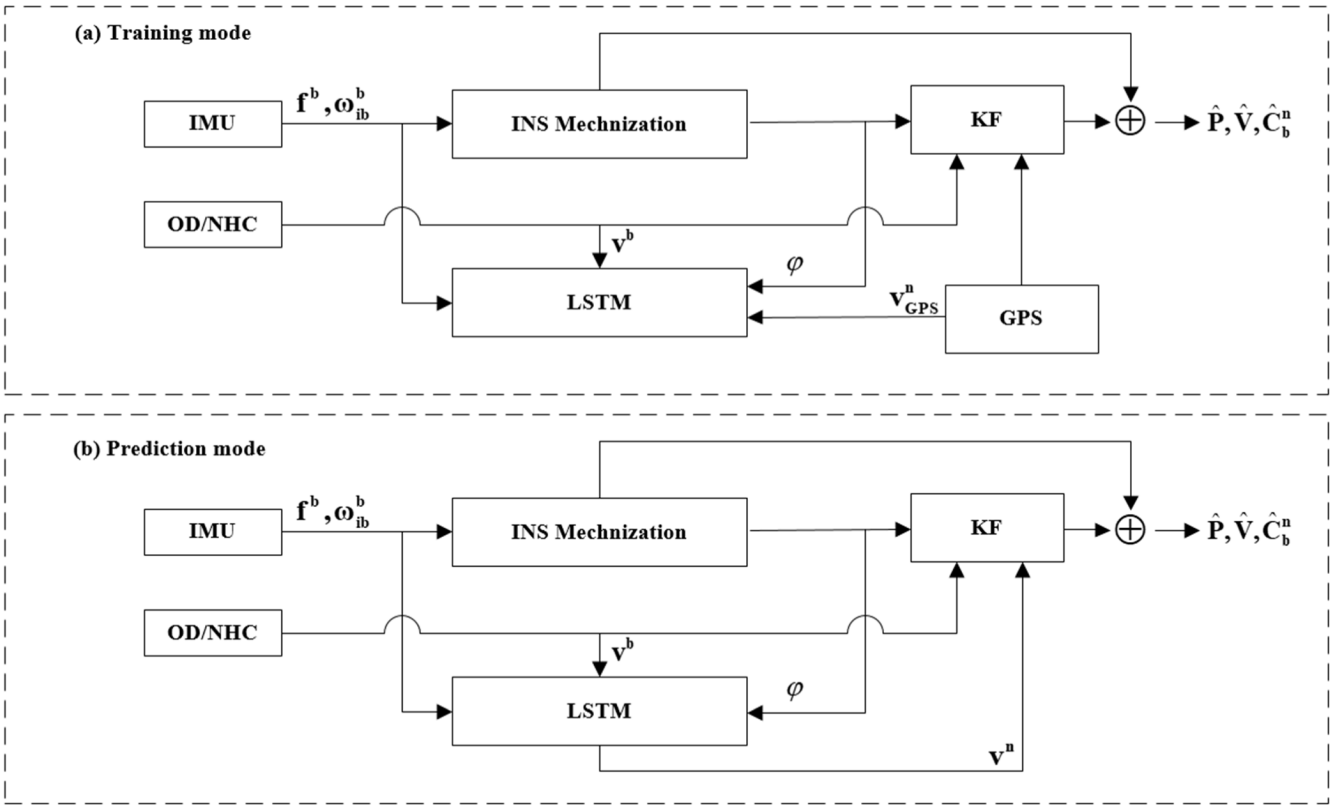

FIGURE 1. Flowchart of the proposed hybrid system of integrated INS/OD/GNSS.

force f^b and the angular rate ω_{ib}^b from the accelerometers and gyro biases, respectively, the azimuth from the INS mechanizations, as well as the body frame velocity formed from the odometer data and NHC. The inertial sensor data is added to the inputs to mimic the vehicle dynamics. The learning targets are the velocities of the east and north directions derived from GNSS. The hybrid integrated system works in the prediction mode during GNSS outages as shown in (b), where the velocity predicted from the trained LSTM NN is used as measurements to estimate the INS errors and therefore to maintain the positioning accuracy without GNSS.

III. DATA FUSION OF MEMS INS, ODOMETER AND GNSS

The reference frames used in this study includes the inertial frame [1], navigation frame, as well as the body frame. The navigation frame is defined as East-North-Up frame, while the body frame is defined as the Right-Forward-Up frame. The reference transformation matrix between inertial frame and body frame, $\mathbf{C_i^b}$, can be calculated as $\mathbf{C_i^n C_n^b}$, where $\mathbf{C_n^b}$ is the transformation matrix from the navigation frame and the body frame, determined by the roll, pitch and azimuth, while $\mathbf{C_i^n}$ is the transformation matrix from the inertial frame to the navigation frame, which is defined in [1]. By considering the error characteristics of the land vehicle navigation, a 15-error states vector, which includes the position errors, velocity errors, and attitude errors in the navigation frame, as well as the accelerometer and gyro biases in the body frame, is chosen as the system states vector as shown in Eq. (1).

$$\mathbf{x} = \begin{bmatrix} \boldsymbol{\delta}\mathbf{r^n} & \boldsymbol{\delta}\mathbf{v^n} & \boldsymbol{\varepsilon}^\mathbf{n} & \boldsymbol{\gamma}^\mathbf{b} & \mathbf{d^b} \end{bmatrix}^T \tag{1}$$

where $\mathbf{x}$ represents the filter state vector, $\boldsymbol{\delta}\mathbf{r^n} = \begin{bmatrix} \delta\phi & \delta\lambda & \delta h \end{bmatrix}^T$ represents the position errors in the navigation frame, $\delta\phi$, $\delta\lambda$ and δh represent the latitude error, longitude error, and height error, respectively, $\boldsymbol{\delta}\mathbf{v^n} = \begin{bmatrix} \delta v_E & \delta v_N & \delta v_U \end{bmatrix}^T$ represents the velocity errors of the navigation frame; δv_E, δv_N and δv_U represent the velocity errors in the east, north and vertical direction, respectively, $\boldsymbol{\varepsilon}^\mathbf{n} = \begin{bmatrix} \varepsilon_E & \varepsilon_N & \varepsilon_U \end{bmatrix}^T$ represents the attitude errors of the navigation frame, ε_E, ε_N and ε_U represent the attitude errors in the east, north and vertical direction, respectively, $\boldsymbol{\gamma}^\mathbf{b} = \begin{bmatrix} \gamma_X & \gamma_Y & \gamma_Z \end{bmatrix}^T$ represents the accelerometer bias vector in the body frame, and γ_X, γ_Y, γ_Z represent the accelerometer biases along X, Y and Z axes, respectively, $\mathbf{d^b} = \begin{bmatrix} d_X & d_Y & d_Z \end{bmatrix}^T$ represents the gyro bias vector of the body frame, and d_X, d_Y and d_Z represent the gyro biases along X, Y and Z axes, respectively.

Based on the perturbation analysis, the error equations for the position error, velocity error, as well as attitude error can be formulated as shown in Eq. (2)–(4) [1].

$$\dot{\boldsymbol{\delta}\mathbf{r^n}} = \mathbf{F_{rr}}\boldsymbol{\delta}\mathbf{r^n} + \mathbf{F_{rv}}\boldsymbol{\delta}\mathbf{v^n} \tag{2}$$

$$\dot{\boldsymbol{\delta}\mathbf{v^n}} = \mathbf{F_{vr}}\boldsymbol{\delta}\mathbf{r^n} + \mathbf{F_{vv}}\boldsymbol{\delta}\mathbf{v^n} + \mathbf{F_{v\varepsilon}}\boldsymbol{\varepsilon}^\mathbf{n} + \mathbf{C_b^n}\boldsymbol{\gamma}^\mathbf{b} \tag{3}$$

$$\dot{\boldsymbol{\varepsilon}}^{\mathbf{n}} = \mathbf{F}_{\boldsymbol{\varepsilon}\mathbf{r}}\delta\mathbf{r}^{\mathbf{n}} + \mathbf{F}_{\boldsymbol{\varepsilon}\mathbf{v}}\delta\mathbf{v}^{\mathbf{n}} + \mathbf{F}_{\boldsymbol{\varepsilon}\boldsymbol{\varepsilon}}\boldsymbol{\varepsilon}^{\mathbf{n}} + \mathbf{C}_{\mathbf{b}}^{\mathbf{n}}\mathbf{d}^{\mathbf{b}} \tag{4}$$

where,

$$\mathbf{F}_{\mathbf{rr}} = \begin{bmatrix} 0 & 0 & -\dfrac{\dot{\phi}}{M+h} \\ \dot{\lambda}\tan\phi & 0 & -\dfrac{\dot{\lambda}}{N+h} \\ 0 & 0 & 0 \end{bmatrix} \quad \text{and}$$

$$\mathbf{F}_{\mathbf{rv}} = \begin{bmatrix} 0 & \dfrac{1}{M+h} & 0 \\ \dfrac{1}{(N+h)\cos\phi} & 0 & 0 \\ 0 & 0 & -1 \end{bmatrix},$$

$\dot{\phi}$ and $\dot{\lambda}$ represent the latitude and longitude rate, respectively.

$$\mathbf{F}_{\mathbf{rr}} = \begin{bmatrix} 0 & 0 & -\dfrac{\dot{\phi}}{M+h} \\ \dot{\lambda}\tan\phi & 0 & -\dfrac{\dot{\lambda}}{N+h} \\ 0 & 0 & 0 \end{bmatrix},$$

$$\mathbf{F}_{\mathbf{vr}} = \begin{bmatrix} 2\omega_e(v_U\sin\phi + v_N\cos\phi) + v_N\dot{\lambda}/\cos\phi & 0 & 0 \\ -2\omega_{ie}v_E\cos\phi - v_E\dot{\lambda}/\cos\phi & 0 & 0 \\ -2\omega_{ie}v_E\sin\phi & 0 & \dfrac{2\gamma}{R} \end{bmatrix},$$

$$\mathbf{F}_{\mathbf{vv}} = \begin{bmatrix} \dfrac{-v_U + v_N\tan\phi}{N+h} & (2\omega_{ie}+\dot{\lambda})\sin\phi & -(2\omega_{ie}+\dot{\lambda})\cos\phi \\ -(2\omega_{ie}+\dot{\lambda})\sin\phi & \dfrac{-v_U}{M+h} & -\dot{\phi} \\ (2\omega_{ie}+\dot{\lambda})\cos\phi & 2\dot{\phi} & 0 \end{bmatrix},$$

$$\mathbf{F}_{\mathbf{v}\varepsilon} = \begin{bmatrix} 0 & f_U & -f_N \\ -f_U & 0 & f_E \\ f_N & -f_E & 0 \end{bmatrix}$$

and f_E, f_N, f_U represent the specific force in the navigation frame, γ represents the normal gravity that varies with the altitude, and $R = \sqrt{MN}$,

$$\mathbf{F}_{\boldsymbol{\varepsilon}\mathbf{r}} = \begin{bmatrix} 0 & 0 & \dfrac{\dot{\phi}}{M+h} \\ -\omega_{ie}\sin\phi & 0 & -\dfrac{\dot{\lambda}\cos\phi}{N+h} \\ \omega_{ie}\cos\phi + \dot{\lambda}/\cos\phi & 0 & -\dfrac{\dot{\lambda}\sin\phi}{N+h} \end{bmatrix},$$

$$\mathbf{F}_{\boldsymbol{\varepsilon}\mathbf{v}} = \begin{bmatrix} 0 & -\dfrac{1}{M+h} & 0 \\ \dfrac{1}{N+h} & 0 & 0 \\ \dfrac{\tan\phi}{N+h} & 0 & 0 \end{bmatrix}, \quad \text{and}$$

$$\mathbf{F}_{\boldsymbol{\varepsilon}\boldsymbol{\varepsilon}} = \begin{bmatrix} 0 & (\omega_{ie}+\dot{\lambda})\sin\phi & -(\omega_{ie}+\dot{\lambda})\cos\phi \\ -(\omega_{ie}+\dot{\lambda})\sin\phi & 0 & -\dot{\phi} \\ (\omega_{ie}+\dot{\lambda})\cos\phi & \dot{\phi} & 0 \end{bmatrix},$$

ω_{ie} represents the earth rotation rate, $\mathbf{C}_{\mathbf{b}}^{\mathbf{n}}$ is the transformation matrix from the body frame to the navigation frame.

By arranging the terms of Eq. (2)-(4), the system dynamic model can be obtained as described in Eq. (5) with the inertial sensor biases modelled as 1st order Gauss-Markov random process [5], [6].

$$\dot{\mathbf{x}} = \mathbf{F}\mathbf{x} + \mathbf{G}\mathbf{w} \tag{5}$$

where

$$\mathbf{F} = \begin{bmatrix} \mathbf{F}_{\mathbf{rr}} & \mathbf{F}_{\mathbf{rv}} & \mathbf{0}_{3\times3} & \mathbf{0}_{3\times3} & \mathbf{0}_{3\times3} \\ \mathbf{F}_{\mathbf{vr}} & \mathbf{F}_{\mathbf{vv}} & \mathbf{F}_{\mathbf{v}\varepsilon} & \mathbf{C}_{\mathbf{b}}^{\mathbf{n}} & \mathbf{0}_{3\times3} \\ \mathbf{F}_{\boldsymbol{\varepsilon}\mathbf{r}} & \mathbf{F}_{\boldsymbol{\varepsilon}\mathbf{v}} & \mathbf{F}_{\boldsymbol{\varepsilon}\boldsymbol{\varepsilon}} & \mathbf{0}_{3\times3} & \mathbf{C}_{\mathbf{b}}^{\mathbf{n}} \\ \mathbf{0}_{3\times3} & \mathbf{0}_{3\times3} & \mathbf{0}_{3\times3} & \boldsymbol{\beta}_{\mathbf{a}} & \mathbf{0}_{3\times3} \\ \mathbf{0}_{3\times3} & \mathbf{0}_{3\times3} & \mathbf{0}_{3\times3} & \mathbf{0}_{3\times3} & \boldsymbol{\beta}_{\mathbf{g}} \end{bmatrix}$$

represents the system dynamic matrix, $\mathbf{G}$ represents the shape matrix of the system noise, $\mathbf{w}$ represents the system noise, $\boldsymbol{\beta}_{\mathbf{a}}$ and $\boldsymbol{\beta}_{\mathbf{g}}$ represent the correlation length matrix regarding to accelerometer and gyros, respectively, and $\mathbf{0}_{3\times3}$ represents the null matrix with size of 3 by 3.

The measurements from the GNSS are the position and velocity in the navigation frame, therefore, the corresponding measurement model is straightforward, and the design matrix $\mathbf{H}_{\mathbf{GNSS}}$ can be described as

$$\mathbf{H}_{\mathbf{GNSS}} = \begin{bmatrix} \mathbf{I}_{3\times3} & \mathbf{0}_{3\times3} & \mathbf{0}_{3\times3} & \mathbf{0}_{3\times3} & \mathbf{0}_{3\times3} \\ \mathbf{0}_{3\times3} & \mathbf{I}_{3\times3} & \mathbf{0}_{3\times3} & \mathbf{0}_{3\times3} & \mathbf{0}_{3\times3} \end{bmatrix}.$$

The body frame velocity formed from the odometer data and the NHC is used as the system measurements, and the corresponding measurement model can be obtained by perturbing the equation $\mathbf{v}^{\mathbf{b}} = \mathbf{C}_{\mathbf{n}}^{\mathbf{b}}\mathbf{v}^{\mathbf{n}}$ as shown in Eq. (6)

$$\delta\mathbf{v}^{\mathbf{b}} = \mathbf{C}_{\mathbf{n}}^{\mathbf{b}}\delta\mathbf{v}^{\mathbf{n}} + \mathbf{V}^{\mathbf{b}}\mathbf{C}_{\mathbf{n}}^{\mathbf{b}}\boldsymbol{\varepsilon}^{\mathbf{n}} = \mathbf{H}_b\mathbf{x} \tag{6}$$

where $\delta\mathbf{v}^{\mathbf{b}}$ represents the velocity errors in the body frame, $\mathbf{V}^{\mathbf{b}}$ is the skew-symmetric matrix of velocity vector in body frame $\mathbf{v}^{\mathbf{b}}$, and the design matrix $\mathbf{H}_{\mathbf{b}} = \begin{bmatrix} \mathbf{0}_{3\times3} & \mathbf{C}_{\mathbf{n}}^{\mathbf{b}} & \mathbf{V}^{\mathbf{b}}\mathbf{C}_{\mathbf{n}}^{\mathbf{b}} & \mathbf{0}_{3\times3} & \mathbf{0}_{3\times3} \end{bmatrix}$.

When GNSS is available, the measurements of the GNSS velocity derived in the navigation frame directly provide the estimates of the system states $\delta\mathbf{v}^{\mathbf{n}}$. Then other error states are estimated from the time derivatives of $\delta\mathbf{v}^{\mathbf{n}}$ [40]. Although the azimuth error ε_U will be drifted when the vehicle maneuvers are weak, as its stochastic observability is poor under such conditions [41], it will not cause the drifting of the INS velocity and position solutions. This is because the INS velocity error and position errors can be directly corrected by the GNSS measurements.

During the GNSS outages, the body frame velocity becomes the only measurement to estimate the INS errors. The measurement model in Eq.(6) can be reformulated as shown in Eq.(7), as shown at the bottom of the next page. Apparently, the attitude error states are coupled with the velocity error states, and none of them can be inferred from the measurements. According to Eq. (3) and (4), the 1st and 2nd time derivatives of the body frame velocity errors are calculated in Eq. (8) and (9), as shown at the bottom of the next page, respectively, with the following assumptions: 1) the vehicle travels on a flat surface that both roll and pitch are

zeroes, 2) the body frame is aligned with the vehicle frame, 3) integration time periods are limited to a fraction of the Schuler period (up to 8minutes) and therefore Earth rotation and Schuler frequency can be neglected; 4) the inherent biases are treated as random constants [38].

The system states can be inferred from the measurements and their time derivatives [40], [41]. As the vehicle usually travels with a relatively constant velocity, we assume the horizontal accelerations f_E and f_N are zeroes for the following error analysis. By examining Eq. (8) and (9), we find that only the accelerometer bias of the vertical axis, γ_Z, and the gyro biases of horizontal axes, d_X and d_Y, can be uniquely estimated from the measurements with no vehicle maneuvers. None of the rest error states, including attitude error state vector, $\boldsymbol{\varepsilon}^{\mathbf{n}}$, velocity error state vector $\boldsymbol{\delta}\mathbf{v}^{\mathbf{n}}$, as well as the horizontal accelerometer biases, γ_X and γ_Y, and gyro bias of vertical axis, d_Z, can be uniquely estimated, although some linear combinations of them can be calculated. Although the horizontal accelerations, f_E and f_N, can enhance the estimation of the azimuth error ε_U and gyro bias d_Z according to Eq. (8) and (9), the local gravity g is usually much greater than those accelerations, which make the stochastic observability of those errors are still poor. As a result, the residual gyro bias d_Z would cause the accumulation of the azimuth error.

The velocity error state vector $\boldsymbol{\delta}\mathbf{v}^{\mathbf{n}}$ can be reformulated based on the measurement model as shown in Eq. (10), as shown at the bottom of the page. Apparently the accumulated azimuth error would cause the drifting in the velocity errors of the east and north directions. As the gyro biases, d_X and d_Y, can be uniquely estimated, it prevents the accumulation of roll and pitch errors. As a result, the velocity error of the vertical direction, δv_U can be maintained converged.

With only the measurement of the body frame velocity, the position and velocity solutions of the east and north directions, as well as the azimuth, will drift during GNSS outages. To maintain the accuracy of the integrated system, the measurements of the velocity of the east and north directions in the navigation frame is required. In the next section, we present a NN-based approach to predict such measurements based on the data collected from the INS, odometer and GNSS.

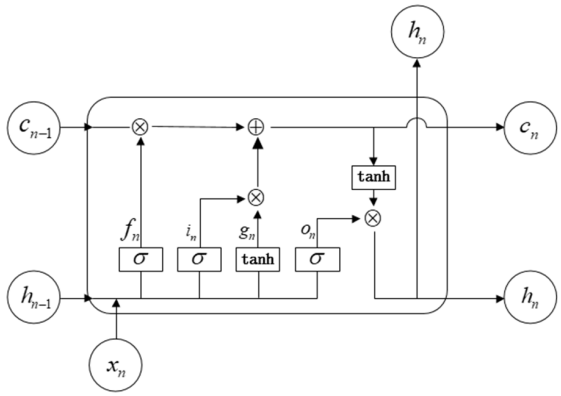

FIGURE 2. Structure of the LSTM NN.

IV. PREDICTION OF VELOCITY MEASUREMENT BASED ON ANN

The LSTM NN can be considered as one of the recurrent neural networks (RNN). Comparing to the traditional neural networks, the LSTM shows advantages in modelling the time correlated sequential data, as it is able to memorize the long-term dependencies of the sequential data.

Therefore, it has been successfully applied to many fields, such as wind speed prediction [42], voice detection [43], pedestrian trajectory prediction [44], traffic flow prediction [45] and navigation [46], [47]. Given the superior ability to model the sequential data, it is employed in this paper to predict the velocity of the east and north directions in the navigation frame with the inputs of INS and odometer data.

Figure 2 illustrates the typical structure of the LSTM NN. With the input sequential data, $\mathbf{x} = (\mathbf{x}_1, \mathbf{x}_2, \cdots, \mathbf{x}_n)$, and the output sequential data, $\mathbf{y} = (\mathbf{y}_1, \mathbf{y}_2, \cdots, \mathbf{y}_n)$, the system input-output equations can be described as shown in Eq. (11)-(17).

$$\mathbf{i}_n = \sigma(\mathbf{w}_{xi}\mathbf{x}_n + \mathbf{w}_{hi}\mathbf{h}_{n-1} + \mathbf{b}_i) \tag{11}$$
$$\mathbf{f}_n = \sigma(\mathbf{w}_{xf}\mathbf{x}_n + \mathbf{w}_{hf}\mathbf{h}_{n-1} + \mathbf{b}_f) \tag{12}$$
$$\mathbf{o}_n = \sigma(\mathbf{w}_{xo}\mathbf{x}_n + \mathbf{w}_{ho}\mathbf{h}_{n-1} + \mathbf{b}_o) \tag{13}$$
$$\mathbf{g}_n = \tanh(\mathbf{w}_{xc}\mathbf{x}_n + \mathbf{w}_{hc}\mathbf{h}_{n-1} + \mathbf{b}_c) \tag{14}$$

$$\begin{bmatrix} \delta v_X \\ \delta v_Y \\ \delta v_Z \end{bmatrix} = \begin{bmatrix} \cos A\delta v_E - \sin A\delta v_N + v_Y\varepsilon_U \\ \sin A\delta v_E + \cos A\delta v_N \\ \delta v_U - v_y \cos A\varepsilon_E + v_y \sin A\varepsilon_N \end{bmatrix} \tag{7}$$

$$\begin{bmatrix} \delta\dot{v}_X \\ \delta\dot{v}_Y \\ \delta\dot{v}_Z \end{bmatrix} = \begin{bmatrix} -g\sin A\varepsilon_E - g\cos A\varepsilon_N + (f_N\cos A + f_E\sin A)\varepsilon_U + \gamma_X + v_Y d_Z \\ g\cos A\varepsilon_E - g\sin A\varepsilon_N + (f_N\sin A - f_E\cos A)\varepsilon_U + \gamma_Y \\ -f_N\varepsilon_E + f_E\varepsilon_N + \gamma_Z - v_Y d_X \end{bmatrix} \tag{8}$$

$$\begin{bmatrix} \delta\ddot{v}_X \\ \delta\ddot{v}_Y \\ \delta\ddot{v}_Z \end{bmatrix} = \begin{bmatrix} -gd_Y + (f_N\cos A + f_E\sin A)d_Z \\ gd_X + (f_N\sin A - f_E\cos A)d_Z \\ -f_N d_E + f_E d_N - v_Y d_X \end{bmatrix} \tag{9}$$

$$\begin{bmatrix} \delta v_E \\ \delta v_N \\ \delta v_U \end{bmatrix} = \begin{bmatrix} \delta v_X\cos A + \delta v_Y\sin A - v_Z\varepsilon_N - (v_X\sin A - v_Y\cos A)\varepsilon_U \\ -\delta v_X\sin A + \delta v_Y\cos A + v_Z\varepsilon_E - (v_X\cos A + v_Y\sin A)\varepsilon_U \\ \delta v_Z - v_N\varepsilon_E + v_E\varepsilon_N \end{bmatrix} \tag{10}$$

$$\mathbf{c}_n = \mathbf{f}_n \odot \mathbf{c}_{n-1} + \mathbf{i}_n \odot \mathbf{g}_n \tag{15}$$
$$\mathbf{h}_n = \mathbf{o}_n \odot \tanh(\mathbf{c}_n) \tag{16}$$
$$\mathbf{y}_n = \mathbf{w}_{hy}\mathbf{h}_n + \mathbf{b}_y \tag{17}$$

where $\mathbf{i}_n$ is the input gating vector, $\mathbf{f}_n$ is the forget gating vector, $\mathbf{o}_n$ is the output gating vector, $\mathbf{g}_n$ is the state update vector, $\mathbf{h}_n$ is the hidden sate of memory cells, $\mathbf{w}_{xi}$, $\mathbf{w}_{hi}$ are the weighting matrix corresponding to input gate, $\mathbf{w}_{xf}$, $\mathbf{w}_{hf}$ are the weighting matrix corresponding to forget gate, $\mathbf{w}_{xo}$, $\mathbf{w}_{ho}$ are the weighting matrix corresponding to output gate, $\mathbf{w}_{xc}$, $\mathbf{w}_{hc}$ are the weighting matrix corresponding to the state update vector, $\mathbf{w}_{hy}$ is the weighting matrix corresponding to hidden state. $\mathbf{b}_i$, $\mathbf{b}_f$, $\mathbf{b}_o$ are the bias vectors corresponding to the input gate, forget gate, and output gate, respectively, $\mathbf{b}_c$, $\mathbf{b}_y$ are the bias vectors corresponding to the state update vector and the output vector, respectively. $\sigma(\cdot)$ represents the standard logistics sigmoid function, and $\tanh(\cdot)$ represents the hyperbolic tangent function.

As shown in the figure, the LSTM structure consists of an input gate, a forget gate, and an output gate. The input gate determines if the input data will be used, and the forget gate decides if the last state will be "forgotten", and the output gate determines if the current state will be propagated [46]. Such network has a gating control mechanism which allows the network to adaptively use the previous data.

In this paper, the body frame velocity formed from the odometer data and NHC, the azimuth from the MEMS INS solutions, as well as the specific force and angular rate from the inertial sensors, which indicates the vehicle dynamics, are chosen as the inputs of the LSTM to predict the velocity of the navigation frame. The GNSS-derived velocities are considered to be the targets. As the data rate of the inertial data is usually much higher than GNSS data rate, the integration of the inertial data over the time span between consecutive GNSS epochs is used, which also reduces the noise level of the raw inertial data, as shown in Eq. (18).

$$\mathbf{x}_i = \begin{bmatrix} \varphi_i & \mathbf{v}^b & \int \mathbf{f}^b & \int \boldsymbol{\omega}_{ib}^b \end{bmatrix}^T \tag{18}$$
$$\mathbf{y}_i = \begin{bmatrix} \mathbf{v}_{GNSS}^n \end{bmatrix} \tag{19}$$

V. FIELD TEST AND RESULTS ANALYSIS

Road tests are conducted with two different MEMS IMUs, namely NAV440 and Crista, to verify the proposed hybrid navigation strategy. For the road test #1, the GNSS receiver from the NovAtel and the NAV440 from the Crossbow Inc. are employed, while the Crista from the Cloud Cap Technology Inc. is employed in road test #2. The SPAN system from the NovAtel, which includes a GNSS receiver and a tactical-grade IMU, HG1700, is used as the reference in both tests. The odometer data is read from the vehicle built-in sensor thorough OBD II interface by using a device, namely CarChip Pro, manufactured by Davis Instruments.

The error characteristics of both MEMS IMUs are summarized in Table 1, which indicates the NAV440 provides the inertial data with higher quality in terms of bias instability and noise density. Both MEMS IMUs has a built-in GNSS pulse per second (PPS) interface which facilitates the accurate time synchronization of IMU and GPS data. The inertial data for the two MEMS IMUs is collected with the data rate of 100 Hz, while the GNSS data and the forward speed data are collected with the data rate of 1 Hz.

TABLE 1. Error characteristics of the NAV440 and Crista.

	parameter	NAV440	Crista
Gyros	Bias instability ($^\circ/h$)	40	1000
	Angular random walk ($^\circ/h/\sqrt{Hz}$)	20	220
	Alignment error($^\circ$)	0.1	1
Accelerometers	Bias instability (m/s^2)	0.01	0.025
	Velocity random walk ($m/s^2/\sqrt{Hz}$)	0.002	0.03
	Alignment error($^\circ$)	0.1	1

Artificial GNSS outages are simulated to verify the ability of the proposed LSTM NN to predict the velocity of the navigation frame, and to evaluate the positioning accuracy of the hybrid system during GNSS outages. The EKF introduced in Section 3 is employed to fuse the low-cost inertial data, the body frame velocity, as well as the GNSS positions and velocities to generate the solutions of the traditional integrated MEMS INS/OD/GNSS system. Moreover, the collected data is also processed by the proposed navigation strategy to generate the solutions of the hybrid system. The reference solutions are obtained by processing the SPAN data using the Inertial Explorer from the NovAtel.

A. RESULTS ANALYSIS OF ROAD TEST #1

Six GNSS outages of 300 seconds are intentionally simulated to the test trajectory. The vehicle dynamics during each outage are summarized in Table 2.

TABLE 2. Vehicle dynamics during each outage.

Outage index	Vehicle dynamics
1	sharp turn, straight line, slight turn,
2	L-shape turn, straight line
3	sharp turn, L-shape turn, straight line, and slight turn
4	sharp turn, L-shape turn, straight line, and slight turn
5	L-shape turn, straight line
6	sharp turn, L-shape turn, straight line, and slight turn

In this study, the first 1000 epochs are used for the training procedure, though 600 epochs are required to achieve the

pre-defined training accuracy (1e-3 in terms of RMSE). The proposed hybrid system works in the predicting mode during the GNSS outages, and the quality of the predicted velocity from the LSTM NN determines the system navigation performance. According to Figure 3 and 4, which illustrate the predicted velocity and the prediction errors during GNSS outage #4, respectively, the predicted velocity from the LSTM NN is highly consistent to the GNSS-derived velocity, and the prediction error (the GNSS-derived velocity is used as references) is maintained within 0.5 m/s.

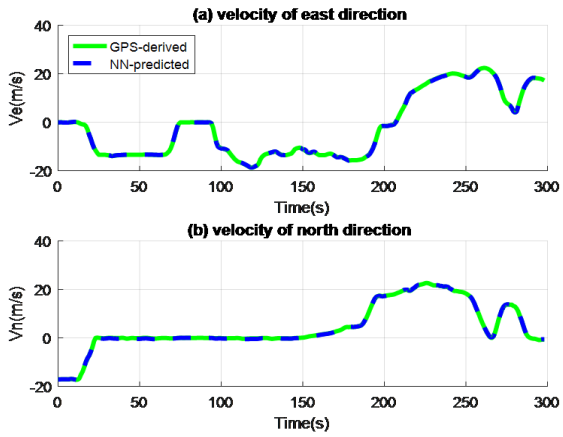

FIGURE 3. LSTM NN-predicted velocity during GNSS outage #4 in road test #1.

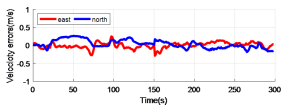

FIGURE 4. LSTM NN-predicted velocity error during GNSS outage #4 in road test #1.

Figure 5 presents the attitude errors of the traditional MEMS INS/OD/GNSS system and the proposed hybrid system during GNSS outage #4. As aforementioned, the poor stochastic observability of the azimuth error and gyro bias in the vertical axis resulted in the accumulated azimuth errors in the MEMS INS/OD/GNSS system during GNSS outages. With the predicted velocity from the LSTM NN, the azimuth is greatly reduced in the hybrid system as shown in the figure. The gyro biases of the horizontal axes can be independently estimated with the body frame velocity measurements, which prevents the accumulations of the roll and pitch errors in the MEMS INS/OD/GNSS system, therefore the predicted velocity from LSTM NN barely affect their estimation accuracy.

Figure 6 illustrates the calculated trajectories for both systems during GNSS outage #4. According to Eq. (10), the accumulated azimuth error leads to the accumulated velocity error, which eventually causes the estimated trajectory of traditional MEMS INS/OD/GNSS system diverged from the reference. Beneficial from the LSTM NN-predicted velocity measurements in the east and north directions, the trajectory

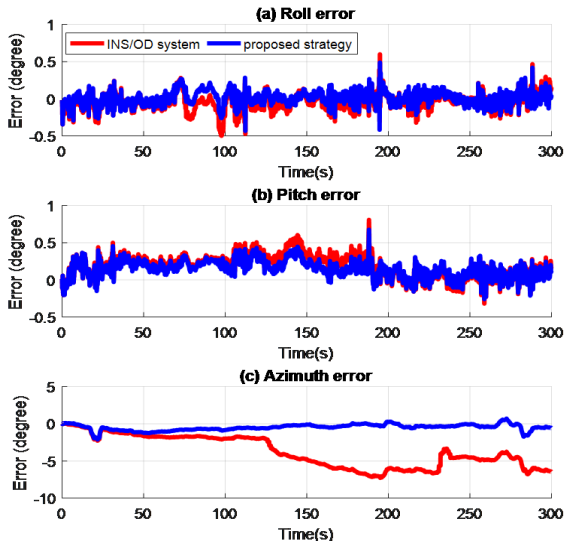

FIGURE 5. Attitude errors of both systems during GNSS outage #4 in road test #1.

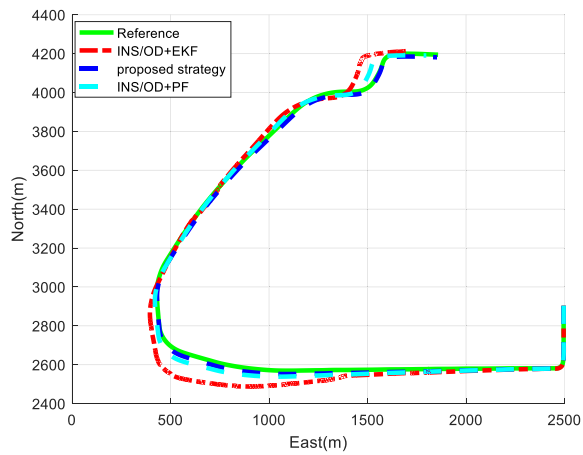

FIGURE 6. Estimated trajectories of both systems during GNSS outage #4 in road test #1.

of the hybrid system is much more consistent to the reference. By differencing with the reference solutions, the corresponding horizontal position and velocity errors for both systems are plotted in Figure 7. The proposed LSTM NN effectively limits the position and velocity error accumulations. The maximum horizontal position errors are reduced to less than 20 m. It is worthy to mention that although the results from other outages also indicate the improvements on the positioning accuracy brought by the proposed strategy, only results of outage #4 is visualized as the obtained positioning errors are the smallest. The PF is also employed to fuse the inertial and odometer data to provide a comparison to the proposed strategy [33]. The obtained trajectory, the horizontal position error and velocity errors during the same outage are illustrated in Figure 6 and 7, respectively. With the predicted velocity measurement from the LSTM NN, the proposed strategy outperforms the PF in terms of positioning accuracy.

TABLE 3. Summary of the RMS and maximum horizontal position errors of both systems for all GNSS outages in road test #1.

Outage index	INS/OD+EKF		Proposed navigation strategy				INS/OD+PF			
	RMS (m)	MAX (m)	RMS (m)	RMS Imprv.	MAX (m)	MAX Imprv.	RMS (m)	RMS Imprv.	MAX (m)	MAX Imprv.
1	278.74	604.18	32.03	88.5%	65.40	89.2%	83.48	70.1%	144.52	76.1%
2	55.04	134.07	31.95	41.9%	43.95	67.2%	40.48	26.5%	104.41	22.1%
3	78.91	185.06	28.82	63.5%	71.30	61.5%	49.56	37.2%	78.30	57.7%
4	83.50	139.70	14.49	82.7%	19.64	85.9%	35.70	57.3%	56.81	59.3%
5	45.31	126.63	20.57	54.6%	27.32	78.4%	30.59	32.5%	47.83	62.2%
6	59.93	196.04	20.05	66.5%	35.37	81.9%	38.55	35.7%	53.55	72.7%

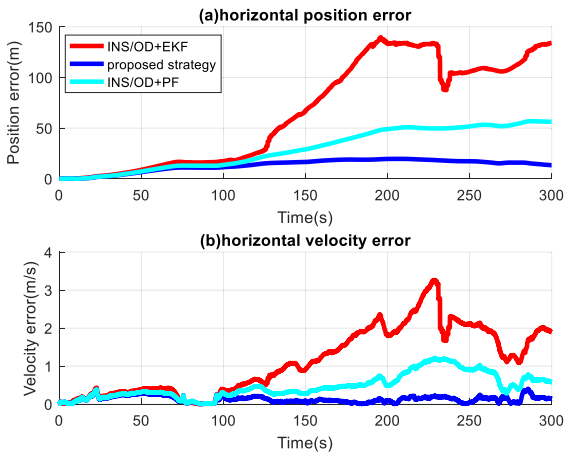

FIGURE 7. Horizontal position and velocity errors of both systems during GNSS outage #4 in road test #1.

Table 3 summarizes the RMS and maximum horizontal position errors for all GNSS outages. The improvements are calculated against to the EKF. Apparently, the proposed LSTM NN greatly reduces the position errors in the hybrid system. Comparing to the EKF method, the average improvements of 66.3% and 77.4% are observed on RMS errors and maximum errors, respectively. It maintains the maximum errors within the range of 19.64-71.30 m (with the RMS error from 14.49 to 32.03 m) during the outage of 300 seconds, as opposed to the maximum error range from 126.63-604.18 m (with an RMS error from 45.31-278.74 m) obtained by the traditional MEMS INS/OD/GNSS system. As shown in Table 3, the proposed system strategy provides the minimum improvements of 41.9% and 61.5% on RMS and maximum errors, respectively. The results obtained from PF are also present in Table 3. Although PF outperforms the EKF in terms of positioning accuracy, the proposed strategy can further reduce the positioning errors with the predicted measurements and.

Although the length of the outages is the same, the obtained positioning errors from the proposed strategy are different for each outage. The positioning errors of the proposed strategy mainly depends on the accuracy of the predicted velocity from the proposed LSTM NN. As aforementioned that the inputs are the accelerometer and gyro outputs, body frame velocity and azimuth, which are strongly related to the random errors of the inertial sensors and vehicle dynamics. According to table 2, the vehicle dynamics for each outage are similar, therefore, the different positioning errors during each outage are mainly caused by the random errors of the low-cost MEMS inertial sensors.

B. RESULTS ANALYSIS OF ROAD TEST #2

Comparing to the NAV440, the higher noise density and bias instability error of the Crista IMU result in greater navigation errors, which would degrade the prediction accuracy of the neural networks. Therefore, shorter GNSS outages are simulated in the second road test. A total of 5 GNSS outages are simulated to verify the feasibility of the proposed navigation strategy with the low-grade Crista IMU. Figure 8 illustrates the predicted velocity from the LSTM NN of the hybrid system during GNSS outage #4, and Figure 9 presents the corresponding prediction errors. Due to the poorer quality of the inertial data from Crista, the discrepancies between the LSTM NN-predicted velocity and GNSS-derived velocity are much greater comparing to the ones for NAV440. Moreover, the prediction accuracy degrades over time.

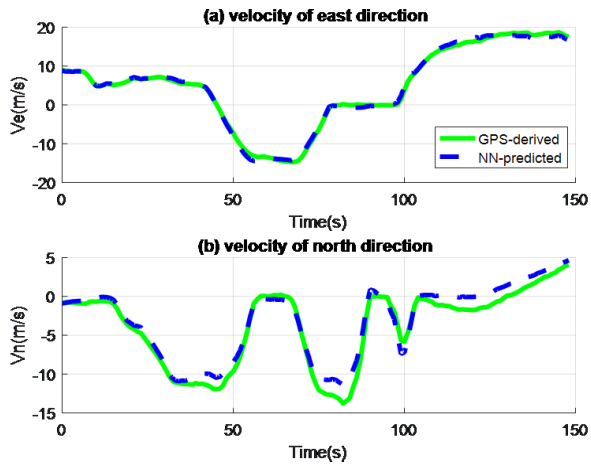

FIGURE 8. LSTM NN-predicted velocity during GNSS outage #4 in road test #2.

Figure 10 presents the obtained attitude errors of both systems during GNSS outage #4. With the measurements of the velocity from LSTM NN, the azimuth error is maintained

TABLE 4. Summary of the RMS and maximum horizontal position errors of both systems for all GNSS outages in road test #2.

Outage index	INS/OD+EKF		Proposed navigation strategy				INS/OD+PF			
	RMS (m)	MAX (m)	RMS (m)	RMS Imprv.	MAX (m)	MAX Imprv.	RMS (m)	RMS Imprv.	MAX (m)	MAX Imprv.
1	199.64	439.09	66.89	66.5%	132.83	69.8%	110.98	44.4%	269.63	38.6%
2	202.54	580.90	87.55	56.8%	253.21	56.4%	135.26	33.2%	353.88	39.1%
3	483.45	1277.23	199.73	58.7%	481.33	62.3%	262.94	45.6%	621.37	51.4%
4	283.79	725.41	23.99	91.6%	58.57	91.9%	109.20	61.5%	358.49	50.6%
5	187.08	286.97	98.81	47.2%	165.44	42.4%	126.87	32.2%	194.41	32.3%

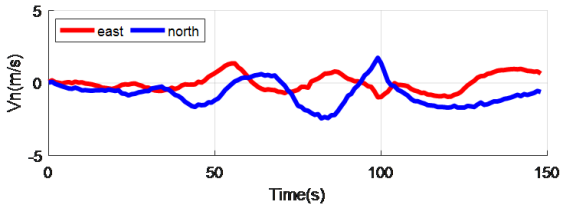

FIGURE 9. LSTM NN-predicted velocity error during GNSS outage #4 in road test #2.

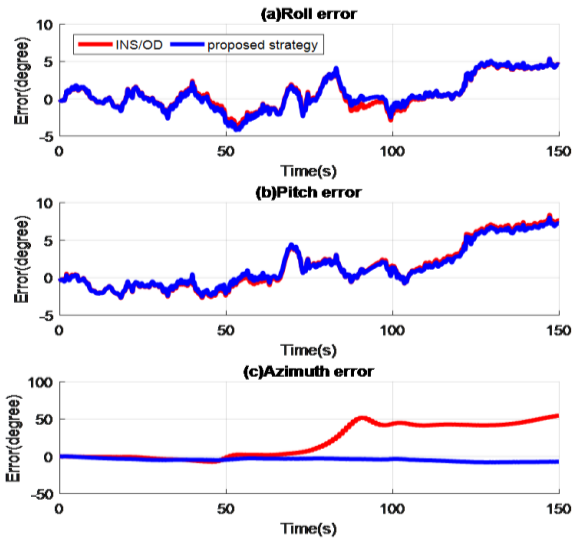

FIGURE 10. Attitude errors of both systems during GNSS outage #4 in road test #2.

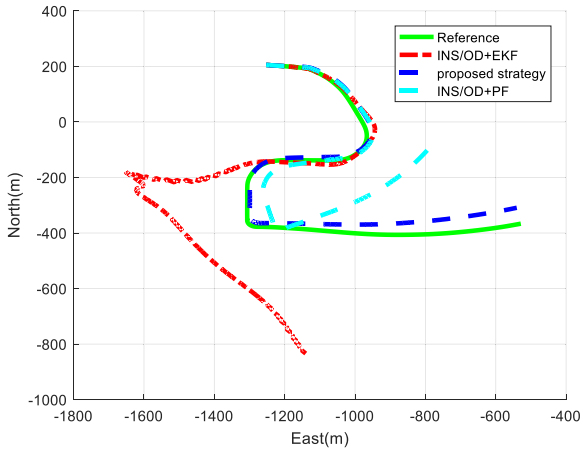

FIGURE 11. Estimated trajectories of both systems during GNSS outage #4 in road test #2.

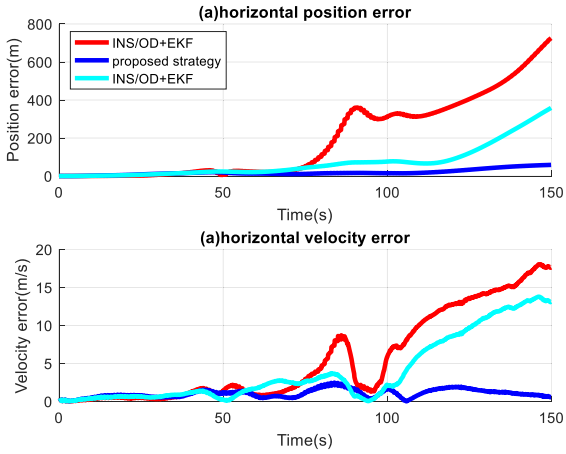

FIGURE 12. Horizontal position and velocity errors of both systems during GNSS outage #4 in road test #2.

within 10 degrees in the hybrid system, whereas it grows to over 50 degrees for the traditional integrated MEMS INS/OD/GNSS system. Similar to the results in road test #1, the roll and pitch errors for both systems are very close.

The corresponding estimated trajectories of both systems are illustrated in Figure 11, followed by the horizontal position and velocity errors given in Figure 12. Apparently, the LSTM NN is able to greatly reduce the navigation errors of hybrid system during GNSS outages, whereas the position errors drift to hundreds of meters for the integrated MEMS INS/OD/GNSS system in 150 seconds. By using PF, the obtained trajectory, position and velocity errors are given in Figure 11 and 12, respectively. Similar to the road test #1, the proposed strategy still outperforms the PF in terms of the positioning accuracy. Table 4 summarizes the RMS and maximum horizontal position errors for both systems. Over all outages, the LSTM NN module provides the average improvements of 64.1% and 64.6% on the RMS and maximum position errors. Based on Table 4, the minimum improvements on RMS and maximum errors are 47.2% and 42.4%, respectively. Comparing to the results in road test #1, the improvements are slightly degraded, as the high-level noise and bias instability of Crista IMU increases the

nonlinear complexity of the input/output functional relationship being modeled. The obtained results by using PF are also summarized in Table 4, which indicates that the proposed strategy offers better positioning accuracy.

VI. CONCLUSION

With the aiding from the odometer, the navigation errors of the inertial system still accumulate over time during GNSS outages. In this paper, we present a hybrid navigation strategy to integrate the MEMS INS, odometer and GNSS to overcome such limitation. The LSTM NN is designed to predict the velocity in the east and north directions of the navigation frame with the inputs being the specific force and angular rate from inertial sensors, the azimuth from the MEMS INS, as well as the body frame velocity formed from both the odometer and NHC. With the LSTM NN-derived velocity, the INS error states can be accurately estimated, and therefore the positioning accuracy of the MEMS INS during GNSS outages is enhanced by the proposed navigation strategy. The road tests are carried out with two different MEMS IMUs, namely NAV440 and Crista, to verify the proposed navigation strategy. Comparing to the traditional integrated MEMS INS/OD/GNSS system based on the EKF, our hybrid approach provides over 60% improvements in terms of RMS and maximum horizontal position errors during GNSS outages.

REFERENCES

[1] D. Titterton and J. Weston, *Strapdown Inertial Navigation Technology*, 2nd ed. Reston, VA, USA: AIAA, 2005.

[2] J. Bernstein, "An overview of MEMS inertial sensing technology," *Sensors*, vol. 20, no. 2, pp. 14–21, Feb. 2003.

[3] N. El-Sheimy, H. Hou, and X. Niu, "Analysis and modeling of inertial sensors using Allan variance," *IEEE Trans. Instrum. Meas.*, vol. 57, no. 1, pp. 140–149, Jan. 2008.

[4] S. Nassar, K.-P. Schwarz, N. El-Sheimy, and A. Noureldin, "Modeling inertial sensor errors using autoregressive (AR) models," *Navigat., J. Inst. Navigat.*, vol. 51, no. 4, pp. 259–268, Dec. 2004.

[5] M. F. Abdel-Hafez, K. Saadeddin, and M. Jarrah, "Constrained low-cost GPS/INS filter with encoder bias estimation for ground vehicles' applications," *Mech. Syst. Signal Process.*, vols. 58–59, pp. 285–297, Jul. 2015.

[6] S. Daneshmand and G. Lachapelle, "Integration of GNSS and INS with a phased array antenna," *GPS Solutions*, vol. 22, no. 1, p. 3, Jan. 2018.

[7] W. Wei, Z. Gao, S. Gao, and K. Jia, "A SINS/SRS/GNS autonomous integrated navigation system based on spectral redshift velocity measurements," *Sensors*, vol. 18, no. 4, p. 1145, Apr. 2018.

[8] B. Cui, X. Chen, X. Yuan, H. Huang, and L. Xiao, "Performance analysis of improved iterated cubature Kalman filter and its application to GNSS/INS," *ISA Trans.*, vol. 66, pp. 460–468, Jan. 2017.

[9] S. Du, W. Sun, and Y. Gao, "MEMS IMU error mitigation using rotation modulation technique," *Sensors*, vol. 16, no. 12, p. 2017, Nov. 2016, doi: 10.3390/s16122017.

[10] Q. Xu, X. Li, and C.-Y. Chan, "Enhancing localization accuracy of MEMS-INS/GPS/in-vehicle sensors integration during GPS outages," *IEEE Trans. Instrum. Meas.*, vol. 67, no. 8, pp. 1966–1978, Aug. 2018.

[11] P. Aggarwal, D. Bhatt, V. Devabhaktuni, and P. Bhattacharya, "Dempster Shafer neural network algorithm for land vehicle navigation application," *Inf. Sci.*, vol. 253, pp. 26–33, Dec. 2013.

[12] V. Havyarimana, D. Hanyurwimfura, P. Nsengiyumva, and Z. Xiao, "A novel hybrid approach based-SRG model for vehicle position prediction in multi-GPS outage conditions," *Inf. Fusion*, vol. 41, pp. 1–8, May 2018.

[13] K.-W. Chiang, A. Noureldin, and N. El-Sheimy, "Multisensor integration using neuron computing for land-vehicle navigation," *GPS Solutions*, vol. 6, no. 4, pp. 209–218, Mar. 2003.

[14] K. W. Chiang, N. El-Sheimy, and A. Noureldin, "A new weights updating method for neural networks based INS/GPS integration architectures," *Meas. Sci. Technol.*, vol. 15, no. 10, pp. 2053–2061, 2004.

[15] N. El-Sheimy, K.-W. Chiang, and A. Noureldin, "Developing a low cost MEMS IMU/GPS integration scheme using constructive neural networks," *IEEE Trans. Aerosp. Electron. Syst.*, vol. 44, no. 2, pp. 582–594, Apr. 2008.

[16] R. Sharaf, A. Noureldin, A. Osman, and N. El-Sheimy, "Online INS/GPS integration with a radial basis function neural network," *IEEE Aerosp. Electron. Syst. Mag.*, vol. 20, no. 3, pp. 8–14, Mar. 2005.

[17] R. Sharaf and A. Noureldin, "Sensor integration for satellite-based vehicular navigation using neural networks," *IEEE Trans. Neural Netw.*, vol. 18, no. 2, pp. 589–594, Mar. 2007.

[18] A. Noureldin, T. B. Karamat, M. D. Eberts, and A. El-Shafie, "Performance enhancement of MEMS-based INS/GPS integration for low-cost navigation applications," *IEEE Trans. Veh. Technol.*, vol. 58, no. 3, pp. 1077–1096, Mar. 2009.

[19] R. Sharaf, M. Reda-Taha, M. Tarboushi, and A. Noureldin, "Merits and limitations of using adaptive neuro-fuzzy inference system for real-time INS/GPS integration in vehicular navigation," *Soft Comput.*, vol. 11, no. 6, pp. 588–598, Jun. 2007.

[20] A. Noureldin, A. El-Shafie, and N. El-Sheimy, "Adaptive neuro-fuzzy module for inertial navigation system/global positioning system integration utilising position and velocity updates with real-time cross-validation," *IET Radar Sonar Navig.*, vol. 1, no. 5, pp. 388–396, 2007.

[21] L. Semeniuk and A. Noureldin, "Bridging GPS outages using neural network estimates of INS position and velocity errors," *Meas. Sci. Technol.*, vol. 17, no. 10, pp. 2783–2798, Oct. 2006.

[22] A. Noureldin, A. El-Shafie, and M. Bayoumi, "GPS/INS integration utilizing dynamic neural networks for vehicular navigation," *Inf. Fusion*, vol. 12, no. 1, pp. 48–57, Jan. 2011.

[23] L. Chen and J. Fang, "A hybrid prediction method for bridging GPS outages in high-precision POS application," *IEEE Trans. Instrum. Meas.*, vol. 63, no. 6, pp. 1656–1665, Jun. 2014.

[24] C. M. Bishop, *Neural Networks for Pattern Recognition*. New York, NY, USA: Oxford Univ. Press, 1995.

[25] J. Li, N. Song, G. Yang, M. Li, and Q. Cai, "Improving positioning accuracy of vehicular navigation system during GPS outages utilizing ensemble learning algorithm," *Inf. Fusion*, vol. 35, pp. 1–10, May 2017.

[26] Y. Yao, X. Xu, C. Zhu, and C.-Y. Chan, "A hybrid fusion algorithm for GPS/INS integration during GPS outages," *Measurement*, vol. 103, pp. 42–51, Jun. 2017.

[27] J. J. Wang, W. Ding, and J. Wang, "Improving adaptive Kalman filter in GPS/SDINS integration with neural network," in *Proc. 20th Int. Tech. Meeting Satell. Division*, 2007, pp. 571–578.

[28] J. Dah-Jing and J. J. Chen, "Neural network aided adaptive Kalman filter for GPS/INS navigation system design," in *Proc. 9th IFAC Workshop*, 2007, pp. 1–7.

[29] J. J. Wang, J. Wang, L. Watts, and D. Sinclair, "Neural network aided Kalman filtering for integrated GPS/INS geo-referencing platform," in *Proc. 5th Int. Symp. Mobile Mapping Technol.*, 2007, pp. 1–6.

[30] X. Li and Q. Xu, "A reliable fusion positioning strategy for land vehicles in GPS-denied environments based on low-cost sensors," *IEEE Trans. Ind. Electron.*, vol. 64, no. 4, pp. 3205–3215, Apr. 2017.

[31] H. Chen, Z. Zhang, Z. Zhou, P. Liu, and Q. Guo, "SINS/OD integrated navigation algorithm based on body frame position increment for land vehicles," *Math. Problems Eng.*, vol. 2018, pp. 1–11, Aug. 2018, doi: 10.1155/2018/5719472.

[32] M. Aftatah, A. Lahrech, and A. Abounada, "Fusion of GPS/INS/Odometer measurements for land vehicle navigation with GPS outage," in *Proc. 2nd Int. Conf. Cloud Comput. Technol. Appl. (CloudTech)*, May 2016.

[33] J. Georgy, T. Karamat, U. Iqbal, and A. Noureldin, "Enhanced MEMS-IMU/odometer/GPS integration using mixture particle filter," *GPS Solutions*, vol. 15, no. 3, pp. 239–252, Jul. 2011.

[34] Z. Gao, M. Ge, Y. Li, Q. Chen, Q. Zhang, X. Niu, H. Zhang, W. Shen, and H. Schuh, "Odometer, low-cost inertial sensors, and four-GNSS data to enhance PPP and attitude determination," *GPS Solutions*, vol. 22, no. 3, p. 57, Jul. 2018.

[35] G. Dissanayake, S. Sukkarieh, E. Nebot, and H. Durrant-Whyte, "The aiding of a low-cost strapdown inertial measurement unit using vehicle model constraints for land vehicle applications," *IEEE Trans. Robot. Autom.*, vol. 17, no. 5, pp. 731–747, Oct. 2001.

[36] I. Klein, S. Filin, and T. Toledo, "Pseudo-measurements as aiding to INS during GPS outages," *Navigation*, vol. 57, no. 1, pp. 25–34, Mar. 2010.

[37] X. Niu, Y. Li, Q. Zhang, Y. Cheng, and C. Shi, "Observability analysis of non-holonomic constraints for land-vehicle navigation systems," *J. Global Positioning Syst.*, vol. 11, no. 1, pp. 80–88, Jun. 2012.
[38] Y. Rothman, I. Klein, and S. Filin, "Analytical observability analysis of INS with vehicle constraints," *Navigat., J. Inst. Navigat*, vol. 61, no. 3, pp. 227–236, Sep. 2014.
[39] A. Li, H. Jiang, J. Zhou, and X. Zhou, "Learning human-like trajectory planning on urban two-lane curved roads from experienced drivers," *IEEE Access*, vol. 7, pp. 65828–65838, 2019.
[40] D. Goshen-Meskin and I. Y. Bar-Itzhack, "Observability analysis of piece-wise constant systems—Part I: Theory," *IEEE Trans. Aerosp. Electron. Syst.*, vol. 28, no. 4, pp. 1056–1067, Oct. 1992.
[41] S. Du, "Self-alignment and calibration of a MEMS IMU: Improving observability and estimability by rotary motions of IMU," *Asian J Control*, vol. 21, no. 4, pp. 1587–1604, 2019, doi: 10.1002/asjc.2032.
[42] H. Liu, X. Mi, and Y. Li, "Smart multi-step deep learning model for wind speed forecasting based on variational mode decomposition, singular spectrum analysis, LSTM network and ELM," *Energy Convers. Manage.*, vol. 159, pp. 54–64, Mar. 2018.
[43] B. Lehner, J. Schluter, and G. Widmer, "Online, loudness-invariant vocal detection in mixed music signals," *IEEE/ACM Trans. Audio, Speech, Lang. Process.*, vol. 26, no. 8, pp. 1369–1380, Aug. 2018.
[44] H. Xue, D. Q. Huynh, and M. Reynolds, "SS-LSTM: A hierarchical LSTM model for pedestrian trajectory prediction," in *Proc. IEEE Winter Conf. Appl. Comput. Vis. (WACV)*, Mar. 2018, pp. 1186–1194.
[45] X. Ma, Z. Tao, Y. Wang, H. Yu, and Y. Wang, "Long short-term memory neural network for traffic speed prediction using remote microwave sensor data," *Transp. Res. Part C, Emerg. Technol.*, vol. 54, pp. 187–197, May 2015.
[46] Y. Zhang, "A fusion methodology to bridge GPS outages for INS/GPS integrated navigation system," *IEEE Access*, vol. 7, pp. 61296–61306, 2019.
[47] W. Fang, J. Jiang, S. Lu, Y. Gong, Y. Tao, Y. Tang, P. Yan, H. Luo, and J. Liu, "A LSTM algorithm estimating pseudo measurements for aiding INS during GNSS signal outages," *Remote Sens.*, vol. 12, no. 2, p. 256, Jan. 2020.

SHUANG DU was born in Sichuan, China, in 1983. He received the B.S. degree in electronics engineering from the Beijing University of Posts and Telecommunications, Beijing, in 2005, and the M.S. and Ph.D. degrees in geomatics engineering from the University of Calgary, Calgary, AB, Canada, in 2011 and 2015, respectively. Since 2017, he has been an Associate Professor with the School of Aeronautics and Astronautics, University of Electronic Science and Technology of China. His current research interests include artificial intelligence, statistical signal processing, and novel sensor-based navigation.

SHU ZHANG was born in Sichuan, China, in 1985. He received the B.S. and M.S. degrees in electronics engineering from Jilin University, Changchun, China, in 2007 and 2009, respectively, and the Ph.D. degree in signal and information processing from the University of Electronic Science and Technology of China, Chengdu, China, in 2014. Since 2015, he has been a Senior Engineer with Sichuan Jiuzhou Electric Group Company Ltd. His current research interests include secondary surveillance radars, signal processing, and artificial intelligence.

XUDONG GAN received the B.S. degree in detection guidance and control technology from the University of Electronic Science and Technology of China, Chengdu, China, in 2019, where he is currently pursuing the M.S. degree in aerospace science and technology. His current research interests include multi-sensor navigation and artificial intelligence.